MODELING THE MECHANISMS UNDERLYING THE FORMATION OF COLLAGEN-MIMETIC TRIPLE HELICES AND MICROFIBRILS

By

VYSHNAVI S. KARRA

A thesis submitted to the

Graduate School – New Brunswick

Rutgers, The State University of New Jersey

In partial fulfillment of the requirements

For the degree of

Master of Science

Graduate Program in Chemical and Biochemical Engineering

Written under the direction of

Dr. Meenakshi Dutt

And approved by

_____

_____

_____

New Brunswick, New Jersey

October, 2017

ABSTRACT OF THE THESIS

Modeling the Mechanisms Underlying the Formation of Collagen-Mimetic Triple Helices and Microfibrils

By VYSHNAVI S. KARRA

Thesis Director:

Dr. Meenakshi Dutt

Collagen is an abundant and integral protein within the body, due to its mechanical strength and elastisticity. These properties arise from the structural hierarchy of collagen, from the peptide strands, to tropocollagen, to microfibrils, to fibers. Understanding the formation mechanisms of collagen can aid in the research of various collagen related disorders, such as heart disease, skin aging, Oseteogenesis Imperfecta, etc. In this study, we simulated three short, simplified collagen peptide strands using the MARTINI coarse grained scheme. Once the tropocollagen was formed, it was replicated five more times and simulated to form a microfibril. Using mathematical equations of a helix, we characterized the tropocollagen to have a curvature (κ) of 0.9237 and a torsion (τ) of 0.6395. The maximum average interaction count occurs between two of the three strands for the tropocollagen at fifteen, suggesting in partial uncoiling of the triple helix. The average interaction counts for the microfibril are around eight, suggesting that the formation mechanism is the individual peptide strands bundling to form a microfibril-like structure, rather than forming tropocollagens and then microfibrils.

Acknowledgements:

Pursuing an M.S. degree within the past year has been quite an experience, and I cannot have done as well as I have without the support and help from the Computational Hybrid Soft Materials Laboratory group members. I would like to thank my thesis advisor, Dr. Meenakshi Dutt, for her guidance and mentoring for the past four years, both as an undergraduate and a graduate student.

It is my privilege to have Dr. Nina Shapley and Dr. Wilma Olson as my committee members. I would like to thank them for accepting my invitation and working to try and find a suitable date for the thesis defense during their busy summer schedules.

I would like to thank my collaborators – Srinivas Mushnoori, Sarah Libring, and Brian Ronan – for their help and guidance throughout this project. I would like to thank Akash Banarjee and Jia Li for their help with the helicity and the interaction counts, respectively.

I would like to thank XSEDE for the computational resources, using Stampede and Stampede2 from Texas Advanced Computing Center (TACC) and Bridges from Pittsburge Supercomputing Center (PSC). In addition, I would like to thank Rutgers Discovery Informatics Institute (RDI2) for providing access to ELF/Caliburn. I would like to thank the creators of NLREG for providing a demonstration version of their program.

Finally, I would like to dedicate this thesis to my younger brother, a special needs individual that always provided the motivation to pursue my academic goals with his cheerful humor and infinite love.

Table of Contents

List of Tables

List of Illustrations

Chapter 1: Introduction

Collagen is one of the most integral proteins in the human body because of its physical properties: 1) elasticity and 2) mechanical strength and stability. In addition to these properties, there are at least sixteen types of collagen. However, the majority of all of the collagen found within the human body are types I, II, and III. Some of the major collagen types are shown below:

Type	Molecular Composition	Structural Features	Representative Tissues
Fibrillar Collagens			
I	$[\alpha1(I)]_2[\alpha2(I)]$	300 nm long fibrils	Skin, tendon, bone, ligaments, dentin, interstitial tissues
II	$[\alpha1(II)]_3$	300 nm long fibrils	Cartilage, vitreous humor
III	$[\alpha(III)]_3$	300 nm long fibrils Often with type I	Skin, muscle, blood vessels
V	$[\alpha(V)]_3$	390 nm long fibrils with globular N-terminal Often with type I	Similar to type I Also cell cultures, fetal tissues
Fibril-Associated Collagens			
VI	$[\alpha1(VI)][\alpha2(VI)]$	Lateral association with type I Periodic globular domains	Most interstitial tissues
IX	$[\alpha1(IX)][\alpha2(IX)]$ $[\alpha3(IX)]$	Lateral association with type II N-terminal globular domain Bound glycosaminoglycan	Cartilage, vitreous humor
Sheet-Forming Collagens			
IV	$[\alpha1(IV)]_2[\alpha2(IV)]$	Two dimensional network	All basal lamina
VII	$[\alpha1(VII)]_3$	Long fibrils	Below basal lamina of the skin
XV	$[\alpha1(XV)]_3$	Core protein of chondroitin sulfate proteoglycan	Widespread Near basal lamina in muscle
Transmembrane Collagens			
XIII	$[\alpha1(XIII)]_3$	Integral membrane protein	Hemidesmosomes in skin

XVII	$[\alpha 1(XVII)]_3$	Integral membrane protein	Hemidesmosomes in skin
Host Defense Collagens			
Collectins		Oligomers of triple helix Lectin domains	Blood, alveolar space
C1q		Oligomers of triple helix	Blood (complement)
Class A scavenger receptors		Homotrimeric membrane proteins	Macrophages

Table 1: Types of collagens with their compositions, primary functions and locations within the body.[19]

Collagen is found within a plethora of systems within the body, with a multitude of functions, ranging from macrophages to the vitreous humor, the transparent tissue with jelly-like consistency that fills the eyeball behind the lens.

Fibrillar collagens are among the most abundant and versatile collagen types. They are made up of long thin fibrils, which are very fine fibers and can then bundle to form fibers. These long thin fibrils arise from a triple helix, where three peptide form a characteristic right handed triple helix. These helices then bundle to form microfibrils that then make up the larger fibrils and collagen fibers. The hierarchy within collagen is the reason for the mechanical strength and stability and the elasticity, which explains the abundance of these types of collagen[19].

For example, researchers at the Oregon State University Linus Pauling Institute found that blood vessels lose their elasticity and stiffen as they age, which could be the root cause of many heart problems that is more prevalent in the older populations.

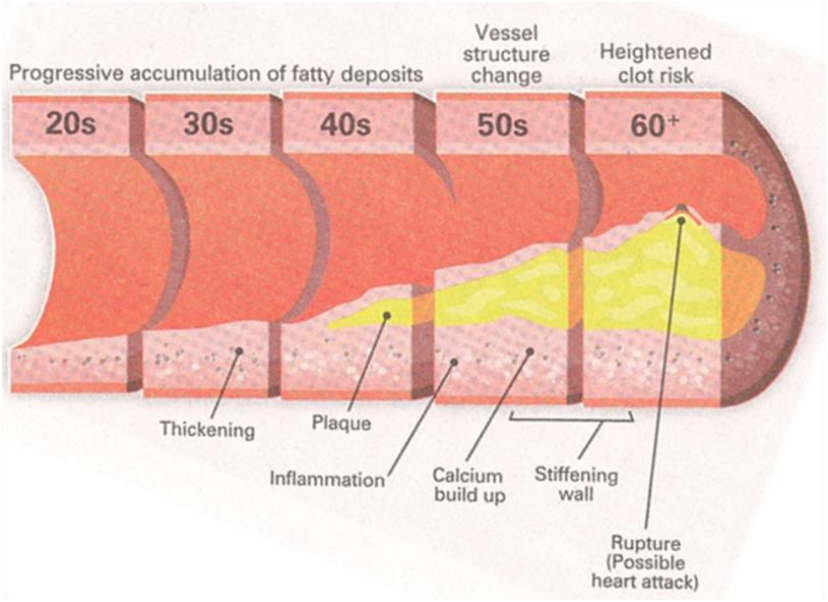

Figure 1: As the arteries age, the walls thicken, causing less blood flow and restricting the contracting and expanding behavior of younger arteries[9].

In younger blood vessels, the walls are smooth muscles that have the capability to contract and expand, in order to pump the blood throughout the body. A thin layer of endothelial cells cover the blood vessel and act as a sensor to regulate this process. However, when blood vessels age, they lose their contracting/expanding capabilities by almost half of that of a younger blood vessel. This loss of function can lead to strokes, hypertension, and heart attacks, which are common causes of death. The researchers at the Linus Pauling Institute found that the collagen in the blood vessels breaks down due to lack of phosphorylation, which leads to a stiffening and thickening of the walls[24].

In another example, recent cosmetics and skincare products use collagen extensively to promote a reversal of wrinkles, one of the most common signs of aging. The skin loses its elasticity which then leads to sagging skins and wrinkles. There are several types of collagen within the skin, most notably type I, III, and VII.

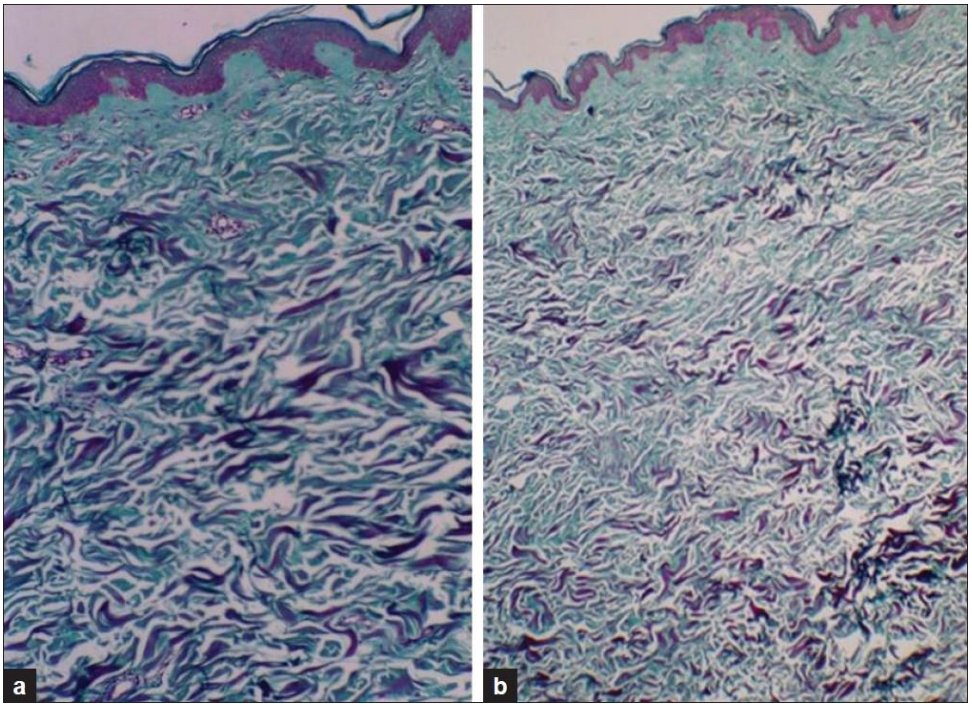

Figure 2: a) young skin showing thick bundles of collagen and b) aged skin showing thinning of the collagen bundles[10]

Aging of the skin has been found as a result of a decrease in the production of collagen type VII[10]. This particular type of collagen is a vital structural component of anchoring fibrils, fibrous structures that are found in the sub-basal laminae of external tissues, such as the skin[26]. In addition to type VII, collagen type I has also been shown to decrease, thus significantly increasing the ratio between type III and type I[10]. Due to these types of studies, many skincare products, such as anti-wrinkle creams from household names such as Olay and L'Oréal, include collagen, hyaluronic acid, retinol, and other molecules that are known to improve the elasticity of the skin.

Sheet forming collagens, such as type IV collagen, form a two-dimensional network, and therefore, it is commonly found in the extracellular matrix (ECM), which primarily provides mechanical support to tissue cells, in addition to various other functions, ranging from cushioning in cartilage to strength in bone. Collagen is one of the

three most abundant components of the ECM, along with proteoglycans and soluble multi-adhesive proteins such as fibronectin. The basal lamina is a special type of ECM, and primarily separates the connective tissue from the epithelial cells. Type IV and laminin, a family of multi-adhesive proteins, form their own two-dimensional networks, which are linked together by entactin molecules, which also helps integrate other components into the ECM, and perlecan molecules, which are multidomain proteoglycans that links the ECM components and cell-surface molecules[19].

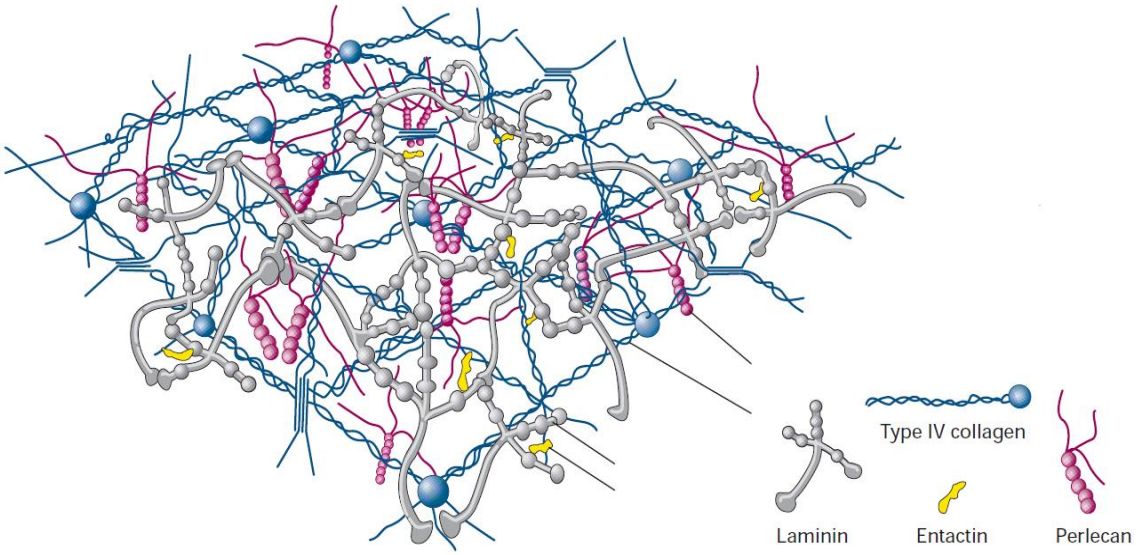

Figure 3: The extracellular matrix is made up of a mesh-like structure of Type IV collagen and laminin, with entactin and perlecan anchoring the mesh-like structure to different tissues depending on the location within the body[19].

Although the biosynthetic pathway of collagen is complex, there have been extensive research done to understand the process. The steps are outlined below:

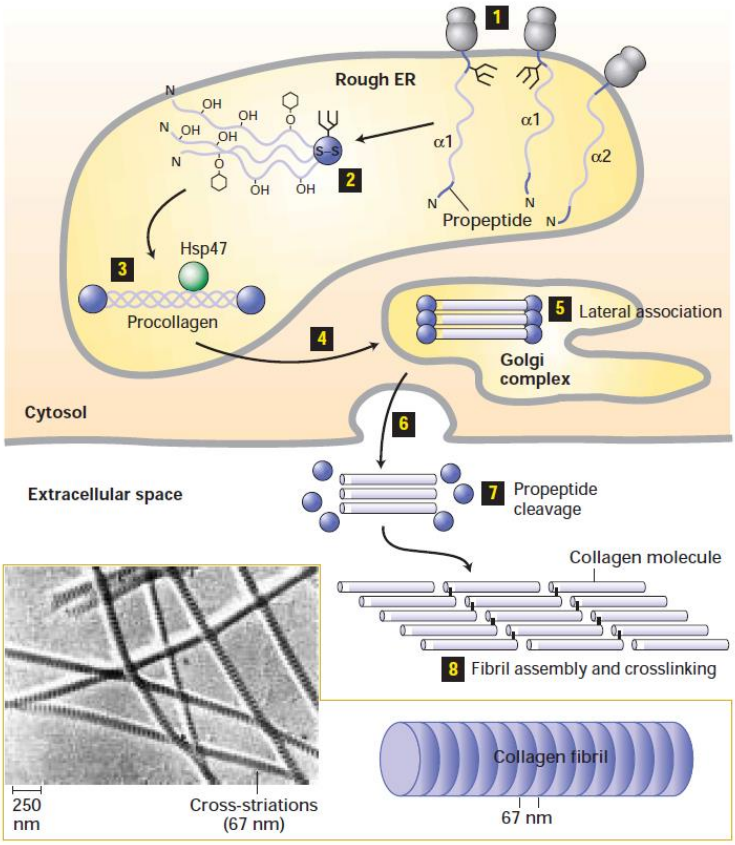

Figure 4: The steps of the biosynthetic process of collagen, which starts in the rough endoplasmic reticulum and ends in extracellular space[19].

Step 1) Ribosomes form the procollagen α strands, the peptide chains that will form a triple helix. These strands have both N-terminal and C-terminal propeptides that then form trimers.

Step 2) Certain residues will be modified and isomerized as necessary (ie. the hydroxylation of some prolines and lysines).

Step 3) This facilitates a zipper-like coiling mechanism, and stabilizes the triple helix, or a tropocollagen

Steps 4 & 5) These tropocollagens are then transported through the Golgi apparatus where small bundles of tropocollagen form.

Steps 6-8) Once these bundles are in extracellular space, the propeptides are cleaved and multiple bundles form cross-links in a staggered array, forming a microfibril[19].

Chapter 2: Background

The abundance of collagen is because of their versatile functionality, primarily due to their mechanical strength and elasticity. These properties arise from the multiscale hierarchy of collagen.

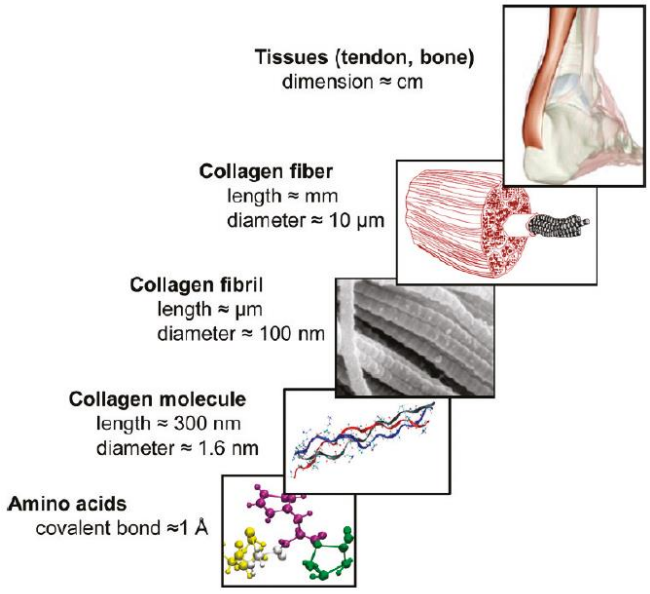

Figure 5: A collagen molecule is made up of 3 peptide chains that are approximately 300 nm long, and twist into a triple helix, aka the tropocollagen. These tropocollagens bundle laterally and longitudinally to form microfibrils and fibrils. Then these fibrils pack into a collagen fiber, which can make up tissue, bone, cartilage, etc[14].

The structure of a collagen molecule is a triple helix, with a length of approximately 300 nm and a diameter of approximately 1.5-1.6 nm. The amino acid sequence is repeating pattern of G-X-Y, where G refers to glycine, the X is typically proline, and the Y is typically hydroxyproline. The location of X and Y can be switched, ie. becoming G-Y-X.[5,14]

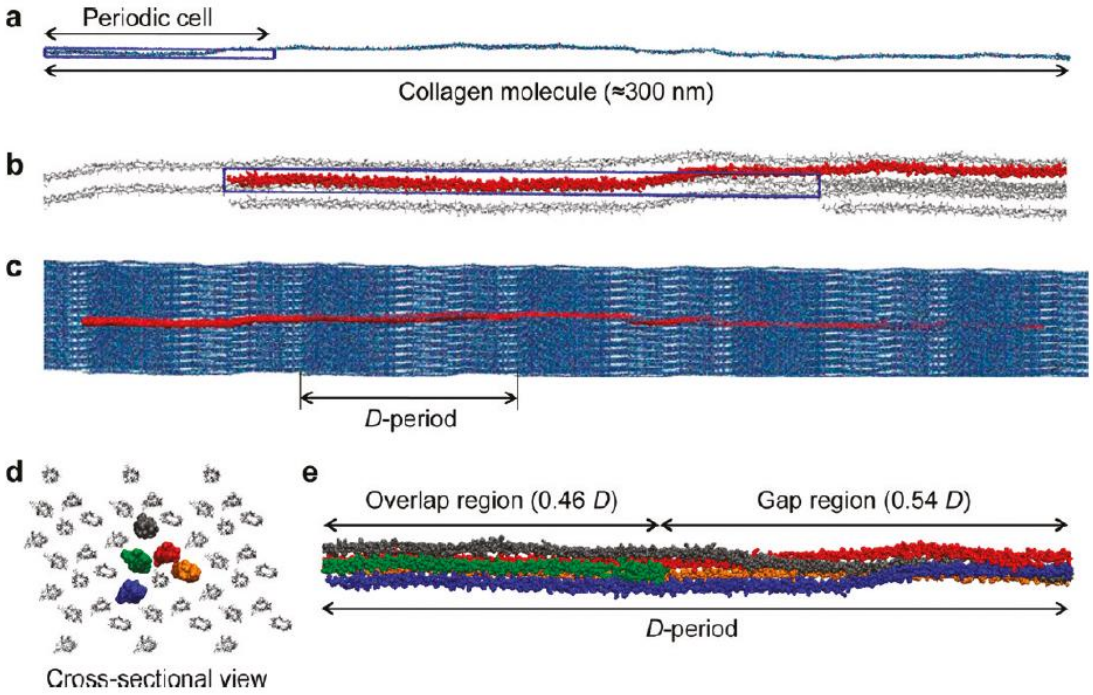

Figure 6: a) full atoms structure of the human collagen type 1. B) periodic images of the unit cell of 1 full length collagen. C) D-banding periodicity seen in AFM images in the microfibril packing. D) quasi hexagonal packing of the microfibril. E) supertwisted right handed microfibril[14]

Microfibrils have periodicity (D) of 67 nm, with an overlap region of 0.46 D (or approximately 31 nm) and a gap distance between the tropocollagens of 0.54 D (or approximately 36 nm). These microfibrils are then bundled to form collagen fibrils. Fibrils have the length in the millimeter range, which are the building blocks of the collagen fiber[5,14]. Fibril formation is typically unipolar, where the molecular polarity is uniform throughout the length of the fibril. Some fibrils are bipolar, where the molecular polarity changes over the length of the fibril. These two types of fibril formation determines the physical and mechanical properties of tissues[17]. Connective tissues, where types I, II, and III collagen is extremely prevalent, is a system of insoluble fibrils, which resist the pulling forces, and soluble polymers, which resist compression forces. These

molecules aggregate in a “quarter stagger” arrays: 75% of each molecule is in contact with neighbors next to each other[29].

When the structural integrity of collagen is defective, a number of diseases can arise: Ehlers-Danlos, osteogenesis imperfecta (OI), scurvy, Caffey disease, etc[6,28]. There are many different types of collagen, depending on the type of tissue, the form, and the function, ranging from types I to XI[17].

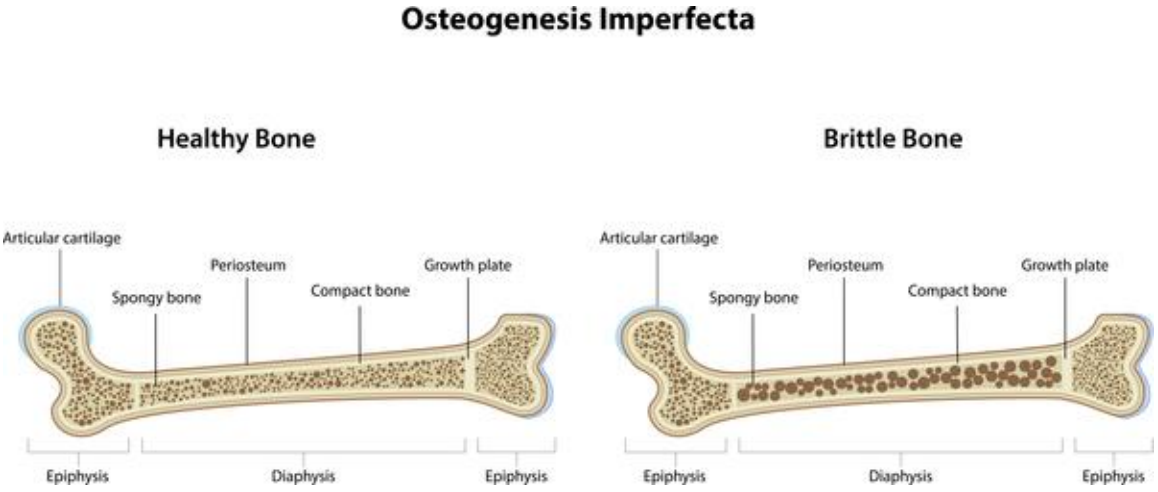

Figure 7: Healthy bones are more dense than brittle bones, due to the lack of fibril packing and a lower concentration of ions[12].

For example, OI – also called “brittle bone disease” – occurs due to mutations in Type I collagen genes, which would affect the cross-links between the lysine resides on two different tropocollagens. Fewer cross-links would lead to poorer fibril packing. These mutations affects the collagen hierarchy at a multitude of scales, from a weakening of intermolecular adhesion to a reduction of fibril strength. Changes in the molecular properties at these levels can cause catastrophic mechanical deterioration of the bones[12].

There have been some progress in the understanding of how the larger structures of collagen fibrils and fibers are formed and how they exhibit mechanical properties of

strength and stability. Gautieri et al[14] validated the experimental data on the mechanical and elastic properties of a collagen microfibril by using an atomistic simulation. However, larger scale simulations of fibrils and fibers would get too computationally expensive. Therefore, the method of coarse-graining would need to be implemented. Buehler et al[5] used atomistic level computer simulations to examine the mechanical and elastic properties of a full-length collagen molecule in order to create a mesoscopic, coarse-grained system.

These types of modeling have been primarily steered molecular dynamics (SMD) in order to test the viscoelasticity of collagen, and calculate the Young's modulus, a ratio between tensile stress ($\sigma(\varepsilon)$) and strain (ε) to calculate the stiffness of a material.

Eq. 1 $$E = \frac{\sigma(\varepsilon)}{\varepsilon}$$

Gautieri et al[13] found that for collagen, the Young's modulus ranges from 6 to 16 Gpa. Ghodsi and Darvish[15] also tested the viscoelasticity of a collagen-mimetic microfibril, composed of two tropocollagens, and found a Young's modulus of 2.24-3.27 Gpa.

However, much of the focus in these computational studies has not been done on the mechanism of the triple helix formation and microfibril formation. Some experimental studies have looked into the kinetics of collagen fibril assembly[22], which have not then been researched in computational studies. This is primarily due to the complexity of the chemistry surrounding collagen microfibril formation, as well as the lack of supercomputing power to simulate multiple full length collagen tropocollagens in a periodic box. With technological advances in supercomputing power, it can be possible to explore these mechanisms in order to understand the full extent of the collagen

hierarchy, which can shed light on how mutations and damage can deform and denature collagen fibers.

Chapter 3: Methodology

3.1 Molecular Dynamics

Computer simulations bridge two different time and length scales, ie. microscopic and macroscopic. They also bridge theory and experiments; theories can be tested using a model, which can then be validated with data from experimental studies. There are many families of simulation techniques that can be utilized in computational studies. Two such families are Monte Carlo (MC) and molecular dynamics (MD). MC tends to favor gas and low density systems, whereas MD tends to favor liquid systems and time-dependent simulations[2]. For this study, as the tropocollagen molecules will be in an explicit solvent, MD was chosen because the focus was on the structure and the dynamics of the tropocollagens and the microfibrils. MC was not chosen because it does not give accurate structural details or have time significance.

Within MD, there are three main ensembles that can be implemented on a system: microcanonical, canonical, and isothermal-isobaric. Microcanonical (NVE) ensembles have a fixed number of molecules, volume, and energy, and corresponds to adiabatic processes. Canonical (NVT) ensembles differ from NVE in that they do not have a fixed energy but instead have a fixed temperature. NVT ensembles employ the use of thermostat algorithms, such as rescaling the velocity, in order to add or remove energy from the MD simulation boundaries to maintain a constant temperature. Isothermal-isobaric (NPT) ensembles require a thermostat as well as a barostat since the pressure, temperature, and number of molecules are fixed[1,8].

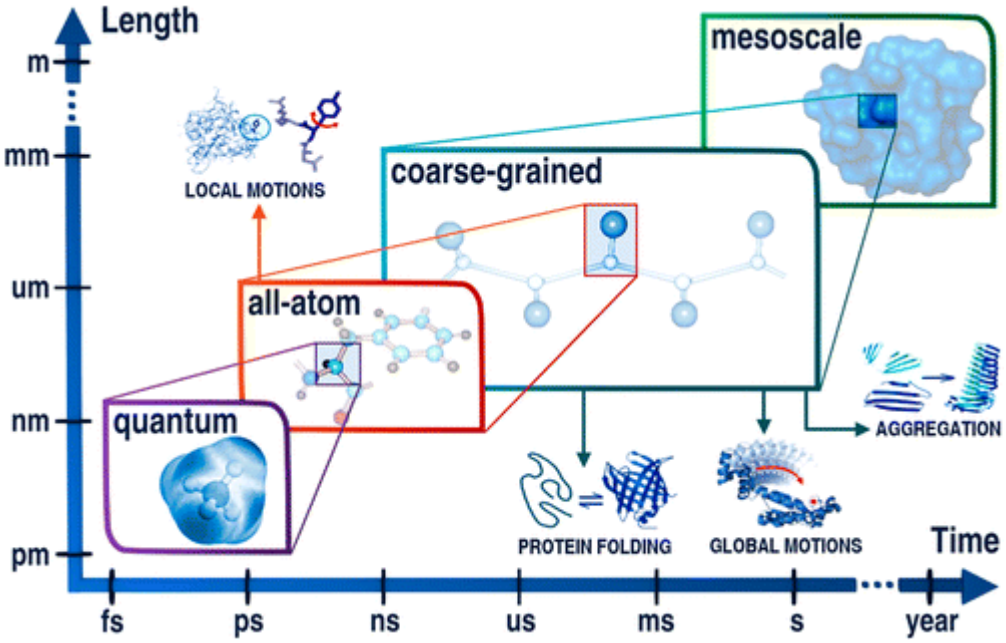

Figure 8: Molecular modeling and it's application ranges with the approximate time and length scales for each. This can be expanded into multi-scale schemes[18].

However, often times simulating all-atom representations of complex systems, such as multiple tropocollagens or microfibrils, can get too expensive, even with the advances in technology. All-atom simulations are primarily limited to small systems and shorter time scales. As a result, coarse-grained representations reduce the computational expense and time needed to model various phenomena. Coarse-grained molecular dynamics (CGMD) simulations can explore larger systems and/or longer time scales. Well-designed CGMD models can reasonably reproduce the structures of all-atom simulations, which creates new opportunities to explore multi-scale modeling, combining the speed of CGMD and the accuracy of all-atom MD[18].

In both all-atom or coarse-grained MD, Newton's equations are solved at every iteration for each molecule *I* within the system.

Eq. 2 $$F_i(t) = m_i a_i(t)$$

Eq. 3 $$v_i(t) = \int a_i\,(t)dt$$

To solve these equations with discrete time steps, where $\Delta t > 0$, the Verlet integration algorithm is utilized to calculate the trajectories. Within this algorithm, the goal is to construct a series of positions at each time step using the previous time step's position. This does not explicitly calculate velocity. This process is repeated for the duration of the simulations.

3.2 Molecular Interaction Potentials

These equations can be represented differently, with potential energy (U).

Eq. 4 $$m_i\ddot{\boldsymbol{r}}_i = \boldsymbol{f}_i \text{ where } \boldsymbol{f}_i = -\frac{\partial}{\partial \boldsymbol{r}_i}U$$

Potential energy can then be split up into non-bonded and bonded interactions. Non-bonded interactions can be represented by a sum of N-body interactions.

Eq. 5 $$U_{non-bonded}(\boldsymbol{r}^N) = \sum_i u(\boldsymbol{r}_i) + \sum_i \sum_{j>i} v(\boldsymbol{r}_i, \boldsymbol{r}_j) + \cdots$$

The first term is the externally applied potential field, which is dropped for fully periodic simulations. The second term is the pair potential, and it is common to neglect higher order interactions (3-body and higher n-body). For complex fluids, it is typically sufficient to use the simplest models to represent the essential physics and dynamics. Continuous and differentiable pair-potentials are commonly used, such as Lennard-Jones and/or Weeks-Chandler-Anderson.

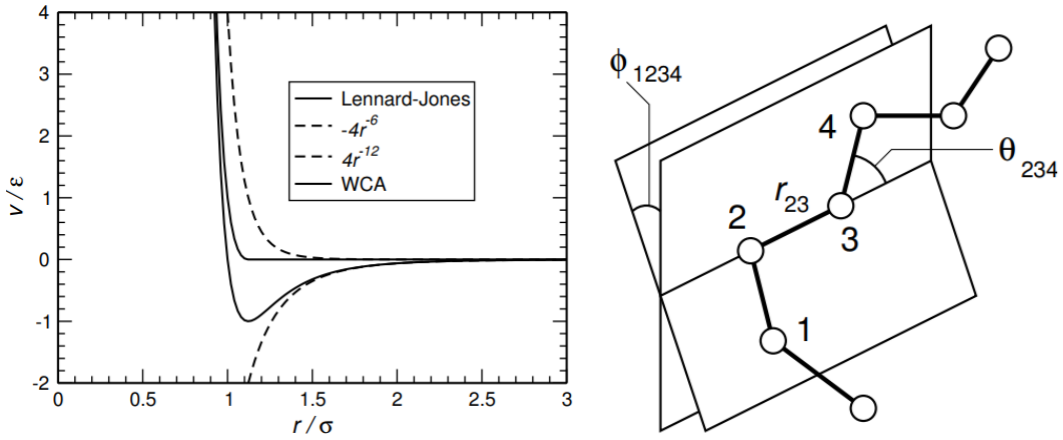

Figure 9: a) the various bonding potentials b) the bonded intramolecular interactions for the bonding potentials[2]

The simplest model for bonding potentials include terms for the bonds, angles and dihedrals within each molecule[2].

Eq. 6 $$U_{intramolecular} = \frac{1}{2}\sum_{bonds} k_{ij}^{r}\left(r_{ij} - r_{eq}\right)^2 + \frac{1}{2}\sum_{angles} k_{ijk}^{\theta}\left(\theta_{ijk} - \theta_{eq}\right)^2 + \frac{1}{2}\sum_{dihedrals}\sum_{m} k_{ijkl}^{\varphi,m}\left(1 + \cos\left(m\varphi_{ijkl} - \gamma_m\right)\right)$$

A major limitation of the Verlet algorithm are that it is not self-starting, because it needs the position at two previous time steps to get the position at the next time step. In order to address this, the leapfrog Verlet algorithm uses a midpoint formula approximation for the velocity, which then is used to calculate the position at the new time step[1].

3.3 Protein Models

There are many different CGMD models for protein simulations, with a wide variety of applications, ranging from protein folding mechanisms to protein structure predictions to protein-protein recognition.

Coarse-grained Model Acronym/Name	**Acronym's Meaning**	**Model Design**	**Example Applications**
AWSEM	**A**ssociated memory, **W**ater mediated, **S**tructure and **E**nergy **M**odel	Up to 3 bead representation: Cα, Cβ, and O.	Ab initio structure preditction of globular proteins; modeling the mechanisms of misfolding and aggregation
Bereau and Deresno	--	Up to 4 bead representation: 3 backbone beads (N, Cα and C') and 1 side chain bead at Cβ	Studying protein folding and aggregation
CABS	**C**-**A**lpha, C-**B**eta, **S**ide chain	Up to 4 bead representation: Cα, Cβ, center of the side chain, and center of the peptide bond.	Ab initio protein structure prediction; ab initio simulations of protein folding
MARTINI	--	Up to 5 bead representation: 1 backbone bead and up to 4 side chain beads	Originally for lipids and has expanded for proteins. Most popular for coarse-grained modeling of membrane proteins in the membrane environment
OPEP	**O**ptimized **P**otential for **E**fficient protein	Up to 6 bead representation: full atom for backbone (N, HN, Cα, C', O) and 1 bead for side	Modeling of proteins, DNA-RNA complexes and amyloid fibril formation; structure prediction of peptides and small proteins

	structure **P**rediction	chains (sans PRO with 3 beads)	
PaLaCe	**Pa**si-**La**very-**Ce**res	2-tier representation – 1 for bonded and 1 for non-bonded interactions	Modeling dynamic fluctuations of folded proteins; protein flexibility prediction
PRIMO	--	Up to 7 bead representation: 3 backbone beads (N, Cα, CO) and 1 to 5 side chain beads	Modeling peptide and small protein structure prediction; been expanded to membrane environments
Rosetta	--	Representation by all backbone atoms, Cβ, and center of side chain.	Widely used for protein structure prediction
SCORPION	**S**olvated **Co**a**r**se-grained **P**rotein **I**nteracti**on**	Up to 3 bead representation: 1 backbone bead and 1 to 2 side chain beads	Initially for scoring protein-protein complexes; later used for protein-protein recognition in a solvated environment
UNRES	**Un**ited **Res**idue	3 bead representation: Cα, peptide group and side chain	Modeling loop structure prediction; protein-DNA interactions; large-scale rearrangements of protein complexes

Table 2: Select coarse grain protein models, with their model design and some applications[18].

The UNRES model is the most classical model of intermediate resolution, with a dependable and a quick reconstruction of the all-atom representation. CABS is another model of intermediate resolution, similar to UNRES, but it differs in its interactions and sampling concepts. PRIMO has a higher resolution than CABS or UNRES, which makes it closer to all-atom representation. The MARTINI model's mapping scheme provides an effective and straightforward method of switching between all-atom and coarse-grained representations, with a plethora of biological applications. The Rosetta model has 2

protein representations: the all-atom and the coarse-grained, combined with the presence of all of the hydrogen atoms. This allows the model to define a confirmation of a protein in with respect to the dihedral space. This is a versatile model for resolution as the program can switch between low and high resolution for a system[18].

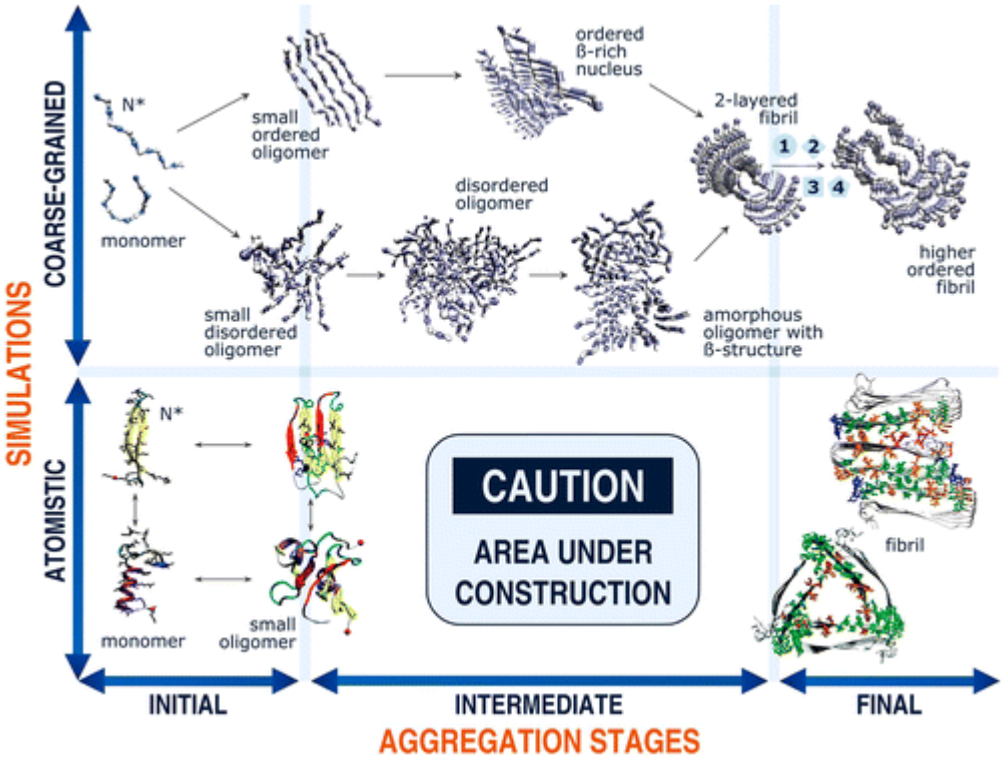

Figure 10: Comparing all-atom and coarse-grained modeling for aggregation processes. The "Under construction" region refers to the current inability of mapping the intermediate aggregation stages to all-atom modeling[18].

Despite the gains made within protein modeling and the mapping that occurs between all-atom and coarse-grained representations, there is still some areas that can be explored. The opportunity to use coarse-grained models to describe aggregation at larger length scales and longer time scales goes beyond the limitations of atomistic simulations[18]. Collagen is one such target for these types of coarse-grained models. Gautieri, Buehler, and their colleagues have started the aggregation process of collagen

peptides into tropocollagens and some microfibril formation. However, mapping the microfibril to fibril networks has not yet been explored, a gateway into understanding the formation of gels from fibrils.

3.4 The Model

The system dynamics within this study was modeled using classical coarse grained molecular dynamics (MD) simulations. The MARTINI coarse graining scheme and force field, developed by Marrink and his colleagues, were utilized because of the extensive application to biochemistry and cell biology.

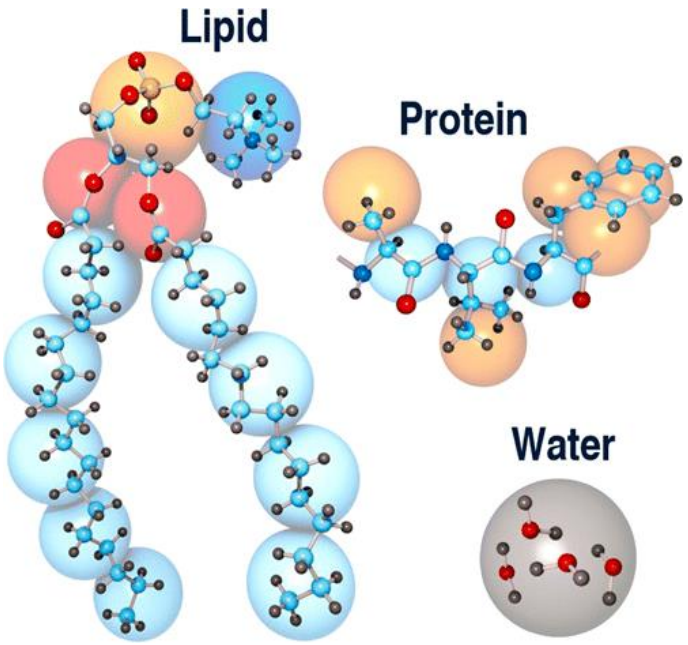

Figure 11: Comparing all atom representation versus the MARTINI coarse grained representation, for a lipid, a peptide chain and water[18].

This is a 4-to-1 mapping scheme, in which four heavy atoms are treated as one interaction center. The number of beads per amino acid is dependent on the steric volume of the amino acid. Therefore, glycine (GLY) is represented by only one bead, whereas proline (PRO) and hydroxyproline (HYP) are represented by two beads. In addition to the size,

there are four types of interactions: polar, nonpolar, apolar, and charged. Within each type, subtypes are distinguished by hydrogen bonding capabilities (donor, acceptor, both, none) and degree of polarity (from 1 as the lowest polarity to 5 as the highest polarity). As a result, an amino acid's specific chemistry is retained.

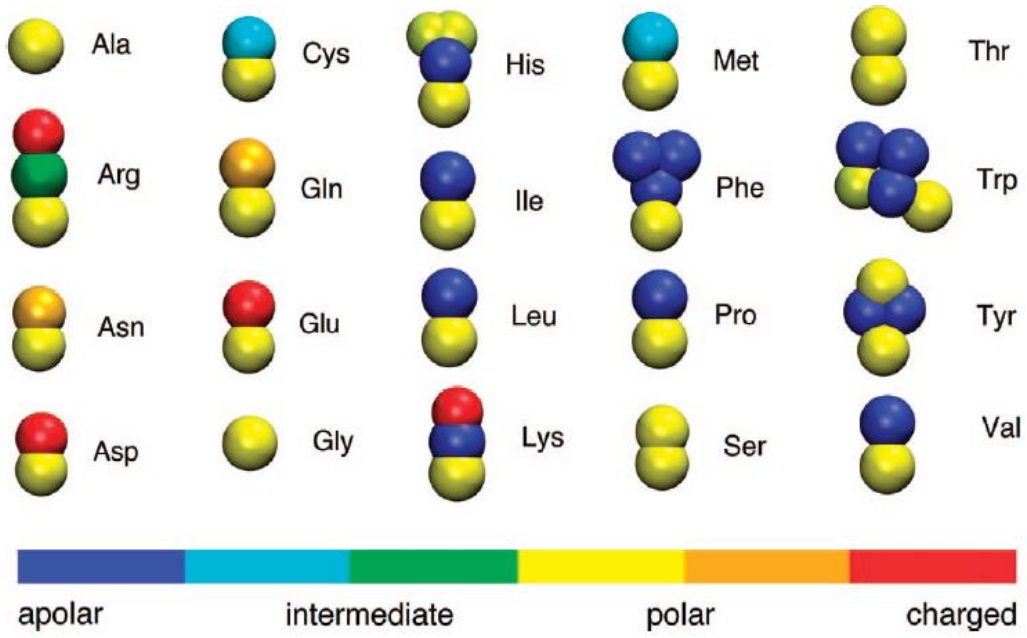

Figure 12: MARTINI mapping for all 20 amino acids, where the names are in the three letter code[21].

Non-bonded interactions of particle pairs *I* and *j* at a distance rij are modeled via the (12, 6) Lennard-Jones (LJ) potential.

Eq. 7 $$V_{LJ}(r_{ij}) = 4\varepsilon_{ij}[(\frac{\sigma_{ij}}{r_{ij}})^{12} - (\frac{\sigma_{ij}}{r_{ij}})^{6}]$$

The strength of the interactions are based on the depth of the attractive well, governed by the parameter ε. Charged groups not only interact via the Lennard-Jones potential, but also via a Coulombic energy function.

Eq. 8 $$V_{Coulomb} = \frac{q_i q_j}{4\pi\varepsilon_0\varepsilon_{rel}r_{ij}}$$

Bonded interactions between bonded sites *I, j, k,* and *l* are described by a set of harmonic potential energy functions for the deformations of the bond length, angles, and dihedrals[20].

Eq. 9 $$V_{bond} = \frac{1}{2}K_{bond}(d_{ij} - d_{bond})^2$$

Eq. 10 $$V_{angle} = \frac{1}{2}K_{angle}[\cos(\varphi_{ijk}) - \cos(\varphi_{angle})]^2$$

Eq. 11 $$V_{dihedral} = K_{dihedral}[1 + \cos(n\psi_{ijkl} - \psi_{dihedral})]$$

The interactions between the different bead types is based on the well depth (ε) of the LJ potential: IX=2.0 kJ/mol, VIII=2.0 kJ/mol, VII=2.3 kJ/mol, VI=2.7 kJ/mol, V=3.1 kJ/mol, IV=3.5 kJ/mol, III=4.0 kJ/mol, II=4.5 kJ/mol, I=5.0 kJ/mol, O=5.6 kJ/mol.

		Q				P					N				C				
Sub		Da	d	a	0	5	4	3	2	1	da	d	a	0	5	4	3	2	1
Q	Da	O	O	O	II	O	O	O	I	I	I	I	I	IV	V	VI	VII	IX	IX
	D	O	I	O	II	O	O	O	I	I	I	III	I	IV	V	VI	VII	IX	IX
	A	O	O	I	II	O	O	O	I	I	I	I	III	IV	V	VI	VII	IX	IX
	0	II	II	II	IV	I	O	I	II	III	III	III	III	IV	V	VI	VII	IX	IX
P	5	O	O	O	I	O	O	O	O	O	I	I	I	IV	V	VI	VI	VII	VIII
	4	O	O	O	O	O	I	I	II	II	III	III	III	IV	V	VI	VI	VII	VIII
	3	O	O	O	I	O	I	I	II	II	II	II	II	IV	IV	V	V	VI	VII
	2	I	I	I	II	O	II	II	II	II	II	II	II	III	IV	IV	V	VI	VII
	1	I	I	I	III	O	II	II	II	II	II	II	II	II	IV	IV	IV	V	VI
N	Da	I	I	I	III	I	III	II	II	II	II	II	II	IV	IV	V	VI	VI	VI
	D	I	III	I	III	I	III	II	II	II	II	III	II	IV	IV	V	VI	VI	VI
	A	I	I	III	III	I	III	II	II	II	II	II	III	IV	IV	V	VI	VI	VI
	0	IV	IV	IV	IV	IV	IV	IV	III	IV	IV	IV	IV	IV	IV	IV	IV	V	VI
C	5	V	V	V	V	V	V	IV	IV	IV	IV	IV	IV	IV	IV	IV	IV	V	V
	4	VI	VI	VI	VI	VI	VI	V	IV	V	V	V	V	IV	IV	IV	IV	V	V
	3	VII	VII	VII	VII	VI	VI	V	V	VI	VI	VI	VI	IV	IV	IV	IV	IV	IV
	2	IX	IX	IX	IX	VII	VII	VI	VI	VI	VI	VI	VI	V	V	V	IV	IV	IV
	1	IX	IX	IX	IX	VIII	VIII	VII	VII	VI	VI	VI	VI	VI	V	V	IV	IV	IV

Table 3: Interaction matrix between all bead subtypes[20].

In its extension to proteins, Monticelli et al[21] set basic parametrization for bond length, angles, dihedrals, force constants, etc. Gautieri et al[11] applied the MARTINI model to collagen amino acids, and characterized HYP according to the mapping and its corresponding parameters. For this study, the tripeptide periodic sequence consists of GLY, PRO, and HYP, based on the characterization by Gautieri et al, with a few changes.

Amino Acid	Backbone bead type	Side chain bead type
GLY	N0*	--
PRO	C5	C2**
HYP	C5	P1

*Table 4: *In Monticelli et al[21], for GLY in helices, the BB bead type was modified to N0 from C5 to account for the properties of a helix. **In MARTINI version 2.0, this was AC2, which is used by Gautieri et al[11], but from version 2.1 this was C2.*

	d_{bond} [nm]	K_{bond} [kJ mol^{-1} nm^{-2}]	φ_{angle} [deg]	K_{angle} [KJ mol^{-1}]$^{\pm}$	$\psi_{dihedral}$ [deg]**	$K_{dihedral}$ [KJ mol^{-1}]**
BB-BB	0.365	100*	98**	1250	60	400
BB-SC	0.300	7500	100	1250	60	400

*Table 5: *Decreased this force constant from the reported value of 200 for a coil by Monticelli et al[21] to introduce more flexibility of the triple helical formation and then the coiling of the tropocollagens in the microfibril formation. ** this were the reported values for a helix. $^{\pm}$Increased this force constant from the reported value of 700 for a helix by Monticelli et al[21] to introduce more rigidity of the PRO and HYP side chain beads for the microfibril formation.*

The major changes from the previous works for these parameters occur with the backbone to backbone force constants. The force constant of the bond was decreased in order to facilitate more flexibility of the assembled tropocollagen for the microfibril formation. Tropocollagens form a right handed coil when assembling into a microfibril. The added flexibility was added to ensure that the triple helix does not undo when coiling into a microfibril[27]. The force constant of the angle was increased in order to increase the

rigidity of the angle and maintain an average distance of 0.5 nm between the PRO and HYP side chain beads[4]. Using these values, we created a Martini coarse grained simplified collagen molecule of only $[GLY\text{-}PRO\text{-}HYP]_{27}$ repeats.

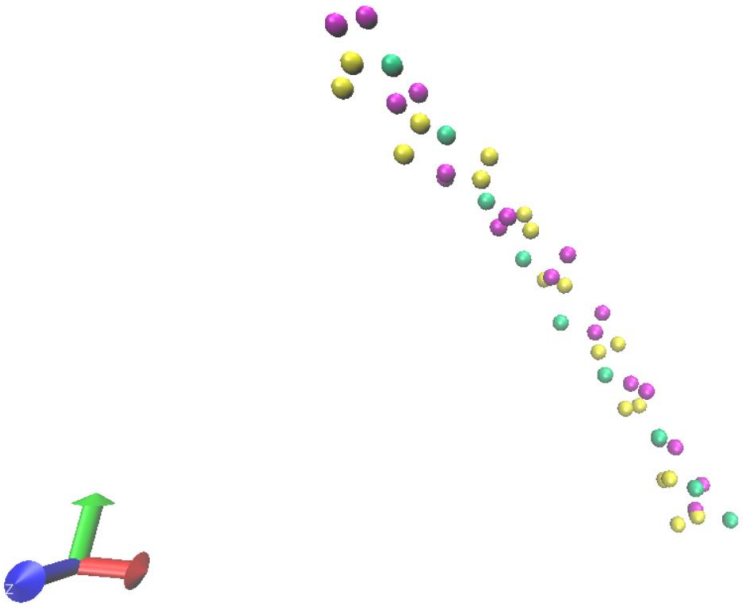

Figure 13: 1 peptide strand that consists of [GLY-PRO-HYP]9 where GLY is in green, PRO is in yellow, and HYP is in magenta

This amounts to 45 MARTINI coarse grained beads for one peptide strand. All of the simulations were run using Groningen Machine for Chemical Simulations (GROMACS), an MD package intended for the simulations of cellular level biology – primarily proteins, lipids, and nucleic acids. GROMACS was originally started at the Department of Biophysical Chemistry at the University of Groningen in the Netherlands. Its goal was to create a parallel computer system specifically for molecular simulations. This particular package was selected because of it is extremely fast at calculating non-bonded interactions, which tend to dominate simulations, It can run on central processing units (CPUs) and graphics processing units (GPUs), allowing for a wider application of the software package without compromising accuracy and speed. The speed varies from 3 to

10 times faster than many other simulation programs. GROMACS's ability to be executed in parallel is another reason why this particular software package was chosen. In addition, the data output files can easily be viewed in software packages such as Visual Molecular Dynamics (VMD), which was used for this particular study[16].

Chapter 4: Triple Helix Simulations

A MATLAB code was created based on the MARTINI coarse-grained mapping of the various amino acids, including HYP. This code wrote the input files of one [GLY-PRO-HYP]$_{27}$ peptide strand, based on an input sequence. As a result, future studies that change the sequence can still utilize this code. This one peptide strand was then simulated using the MARTINI force field version 2.2. The system was equilibrated, using the steepest descent algorithm, for about 1 ns with a time step of 1 fs in an extremely large periodic box (30x30x30 nm^3), to ensure a stable structure. This particular equilibration occurred without any water molecules because one of the goals was to ensure that the input parameters did not cause the simulation to blow up. The other goal was to measure the length of the peptide strand, for the next simulations. With a large periodic box, the inclusion of water molecules will greatly slow down the computational speed. In addition, the presence of only one peptide strand in water would not yield any significant results for this particular study. In addition, the time step is fairly small to track to the changes in the potential energy as the

The total length of the peptide strand was found to be approximately 6.9 nm. This length is particularly useful in calculating the size of the periodic box for the tropocollagen simulations. A common guideline for computer simulations is to have a periodic box size that is about 1.5 times larger than the length of the molecule. This is to ensure that one end of the molecule does not interact with its other end through the periodic boundary walls. As a result, the tropocollagen simulations had a periodic box size of 11x11x11 nm^3. Then the one peptide strand was replicated two more times, to have a total of 3 peptide strands, with a total of 135 MARTINI coarse-grained beads,

placed randomly within the periodic box. Once this was solvated with water and positive ions, there were approximately 10,600 water beads and enough positive ions to ensure that the charge of the system is neutral.

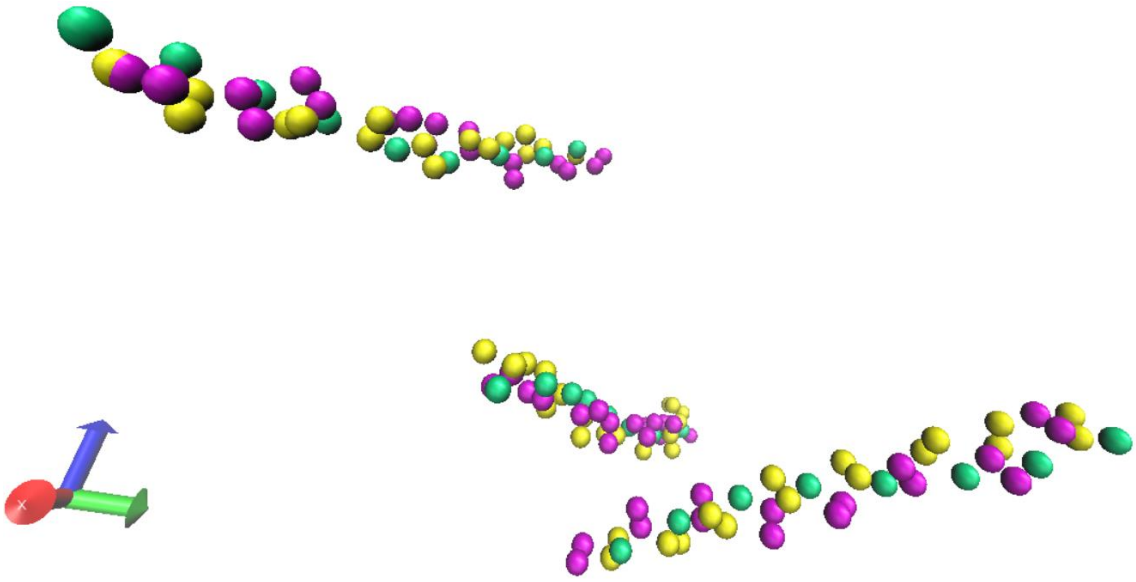

Figure 14: A zoomed-in view of the 3 peptide strands in solvent, where GLY is green, PRO is yellow, HYP is magenta.

Sodium ions were chosen due to the polarity of the HYP beads and the interactions between them and the water beads. The energy of this system was minimized for 1 ns with a time step of 1 fs, similar to how the energy of the 1 peptide strand was minimized earlier. Then, the Molecular Dynamics simulation ran for 320 ns with a time step of 8 fs. Typically, the time steps for coarse-grained molecular simulations are around 20 to 30 fs. However, with the presence of dihedrals, the time step is often around 10 fs, due to the extra constraints that dihedrals present to the calculations.

The MD simulation was done in the GROMACS package using the standard integrator, a leap-frog algorithm for integrating Newton's equations of motion[16]. This system operates at NVT, with the temperature at 310 K, which is approximately 37°C or

the average body temperature. The temperature coupling for the themostat was done using velocity rescaling, which is similar to the Berendsen thermostat. This allows for random seeds to be set manually. The Parrinello-Rahman barostat was also applied, in order to keep the temperature constant[20].

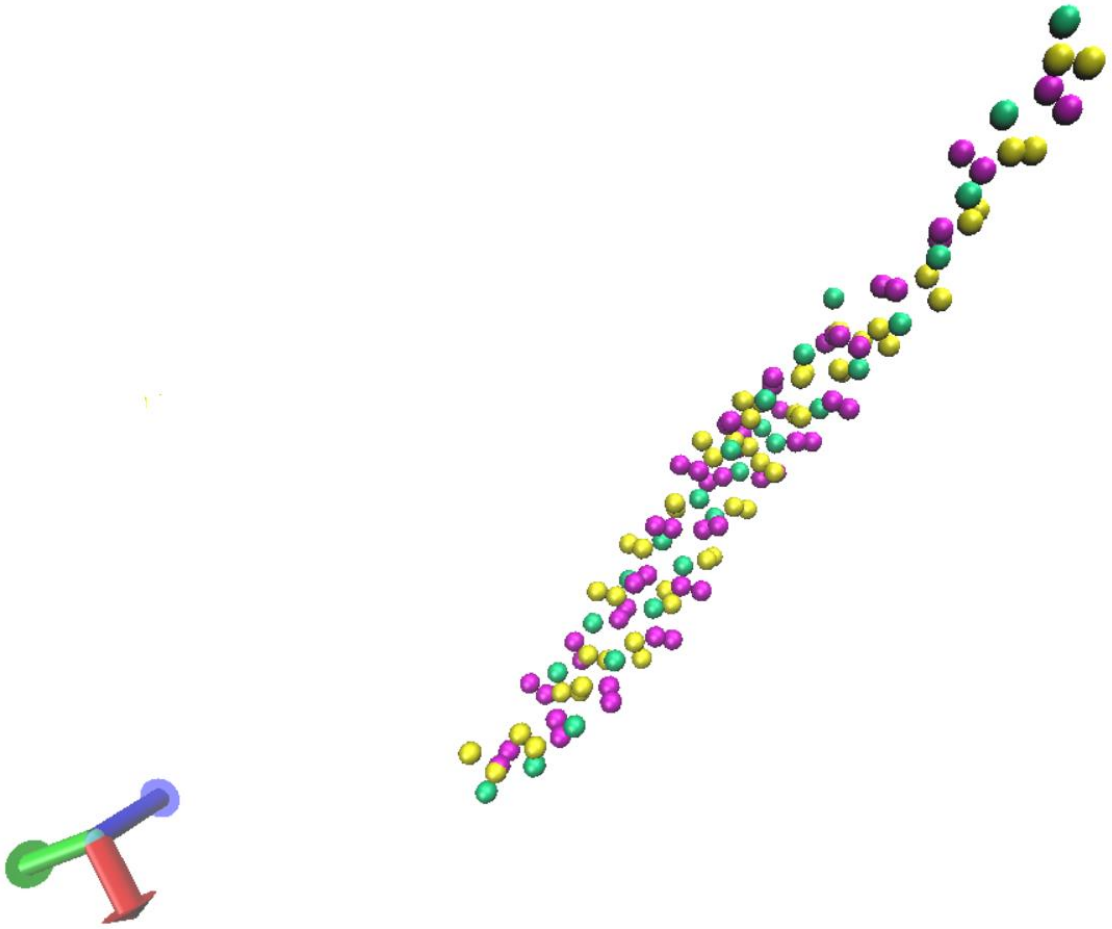

Figure 15: After 120 ns, the tropocollagen appears to have formed a complete triple helix. It is unclear at this point of the simulation whether it is stable.

After 120 ns are completed in the simulation, the tropocollagen is in a complete triple helix-like configuration. The completeness refers to the three strands being twisted around throughout the length of the tropocollagen. To test the stability of this tropocollagen, the system was simulated for another 200 ns. Within these 200 ns, the

tropocollagen appears to uncoil and then re-coil. However, from the 280 ns mark onwards in the simulation, the tropocollagen is no longer a complete triple helix. In other words, the three strands are in a helical configuration, however it is only the ends of the strands that are a true triple helix. It appears to have partially uncoiled, and has remained that way until the simulation ended at 320 ns. We are currently in the process of running seven more seeds to see if the uncoiling behavior is a reproducible phenomenon.

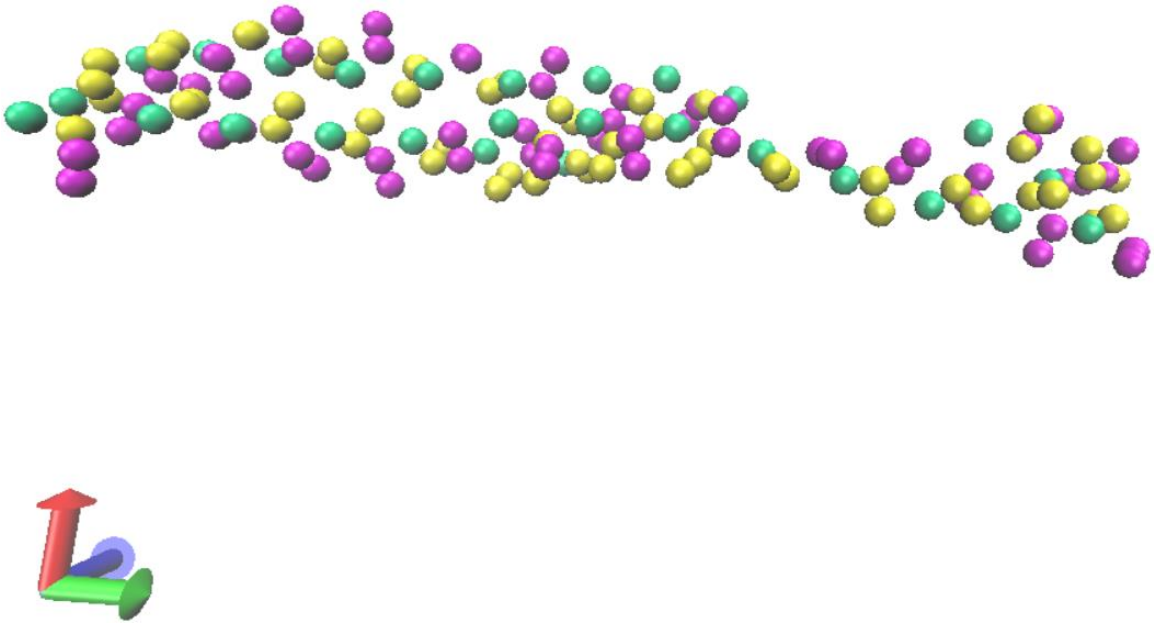

Figure 16: After 320 ns, the tropocollagen is no longer a complete triple helix. The 3 strands are in a helical configuration, however they are not twisted together throughout the entire length.

It is unclear whether further simulation of the system would cause the triple helix to become complete once again, and whether this behavior is only for shorter lengths of collagens. This dynamic can be explored in future studies.

Chapter 5: Microfibril Simulations

Once a stable triple helix was formed, it was then replicated five more times, to get a total of six triple helices or 18 peptide strands. With the increase of strands, the periodic box size was increased to 20x20x20 nm^3, resulting in ~63000 water beads and a corresponding increase in positive ions.

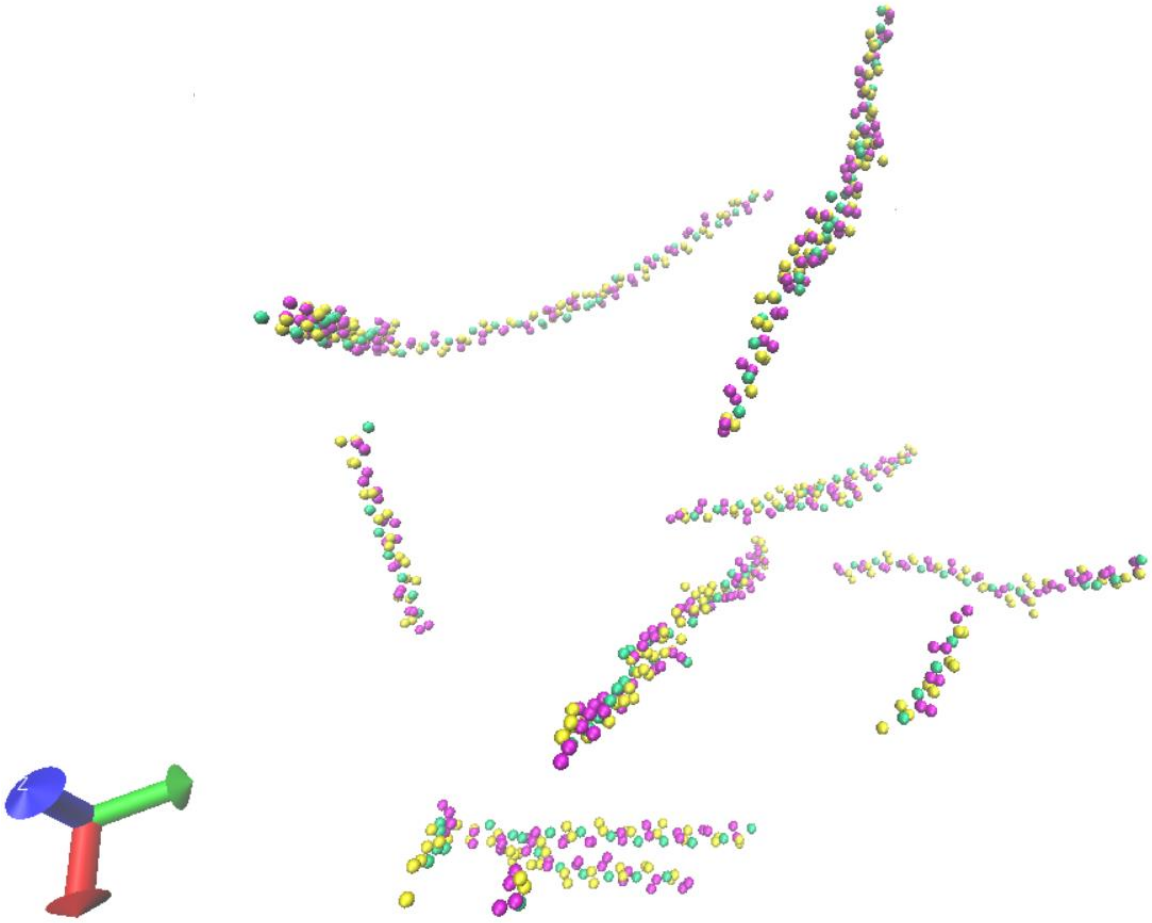

Figure 17: The initial configuration of the 6 tropocollagens within the periodic box.

These strands were then simulated for approximately 1.1 μs, using the same MD simulation parameters as before with the tropocollagen simulations. The increase in simulation time is because of the larger number of particles. For the tropocollagen simulation, there were only approximately 10,600 particles in total. For the microfibril

simulation, there were nearly six times as many particles. The increase in the number of particles would increase the number of non-bonded interactions that can occur. Thus, the increase in simulation time.

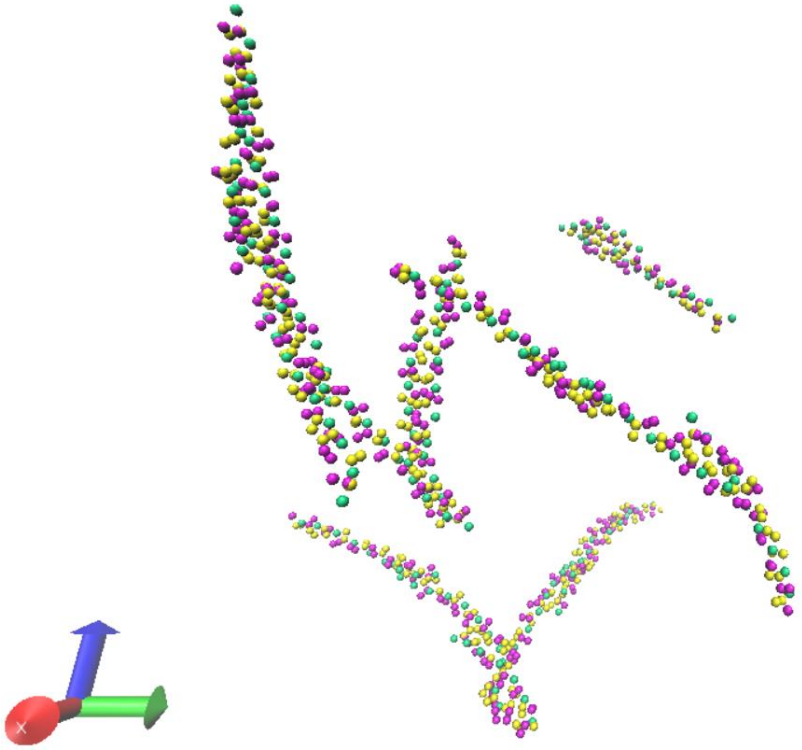

Figure 18: After 560 ns, the 6 tropocollagens are starting to move closer, and starting to assemble.

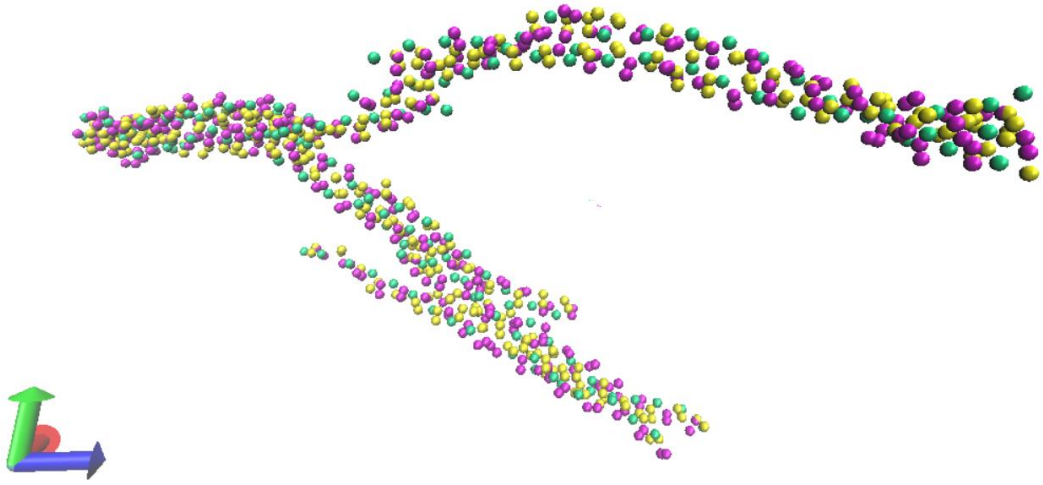

Figure 19: A microfibril is almost completely formed after nearly 1.1 μs of simulation.

After nearly 1.1 μs of simulation, an almost complete microfibril-like bundle is formed. It spans nearly the entire periodic box's diagonal, and the strands appear to twist around each other. It is unclear at this point whether those strands are forming tropocollagens and then those tropocollagens are forming a microfibril, or the strands are all twisting around each other to form a microfibril-like structure. Future studies may be able to characterize the structures formed to determine the correct mechanism of the assembly.

Chapter 6: Results & Discussion

6.1 Helicity of the Triple Helix

First, we had to ensure that the tropocollagen is indeed a triple helix, or at least in some sort of helical configuration. Based on the VMD images, it qualitatively seems to be a triple helix, especially when it is fully twisted. Even when it is partially uncoiled, it still appears to be in a helical configuration. However, the characteristics of a helix can be quantified. The tilt of each of the strands within the triple helix was calculated, using the Nonlinear Regression Analysis Program (NLREG) demonstration code provided by Phillip H. Sherrod. NLREG works by taking the data and attempting to find the curve of best fit for the data provided. In order to do so for a 3-dimensional molecule, the data had to be independent of one of the 3 directions (x, y, z). This is done by setting one direction equal to zero (ie. z=0)[23].

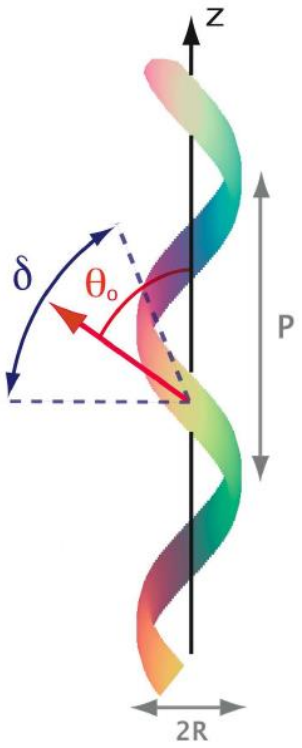

Figure 20: For a collagen helix, the mean angle (θ) is approximately 57°, and δ is the disorder width, or the range in which the angle could reside. Therefore, the range is between 23° and 90° for a collagen helix[30].

The regression was done for each strand each of the three directions, by setting x=0, then y=0, then z=0, to figure out which 2-dimensional projection would work best with the data. Therefore 9 different regressions were performed, and it was found that a projection on the XY plane worked best for this particular tropocollagen.

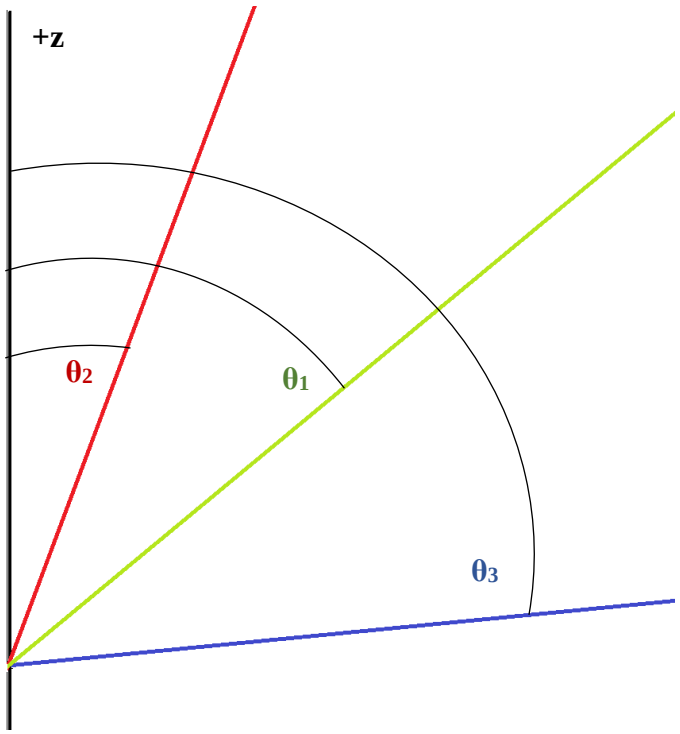

Strand 1 (green)	87.9790°
Strand 2 (red)	26.5993°
Strand 3 (blue)	55.6253°

Figure 21: Schematic of the angles calculated for the 3 peptide strands. The table shows the calculated angles from the NLREG code.

These angles fall within the range of angles for a collagen helix (23° to 90°), based on experimental data[30]. This characterization is not enough to show that a stable triple helix has been achieved. To further quantify the tropocollagen, we went back to the literature. A collagen triple helix has an axial rise of 2.86 nm, a diameter of approximately 1.5 nm, with the PRO ring on one strand and the HYP ring on another strand being about 0.5 nm apart. Notably, collagen can either be in a “relaxed” triple helix or a “rigid” triple helix. The “relaxed” form is the 10/3 (10 amino acids per 3 turns) and the “rigid” form is the 7/2 (7 amino acids per 2 turns)[4].

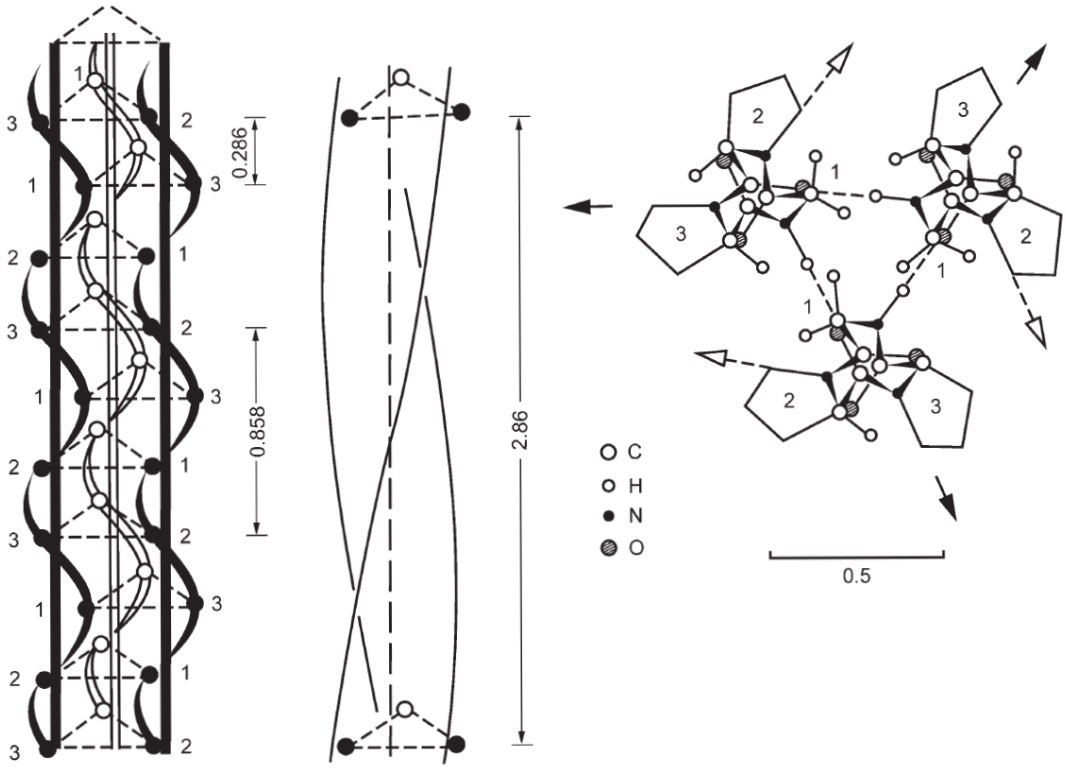

Figure 22: A collagen triple helix parameters, where the axial rise is 2.86 nm and the distance between the PRO ring and the HYP ring is 0.5 nm[4].

In addition, a helix can be mathematically represented by a set of three parametric equations.

Eq. 12 $x = rcos(t)$

Eq. 13 $y = rsin(t)$

Eq. 14 $z = ct = (\frac{axial\ rise}{2\pi})t$

For the reported values of a collagen triple helix, these parametric equations then become:

Eq. 15 $x = (0.75)cos(t)$

Eq. 16 $y = (0.75)sin(t)$

Eq. 17 $z = (0.4551)t$

Based on these equations, it is possible to calculate the curvature (κ) and torsion (τ) of a helix. Curvature is the rate of change of a unit vector along the direction of motion along the curve. Essentially, it is the rate at which a curve bends. The radius of curvature is 1/ κ. Torsion is the magnitude of the rate at which a curve twists around an axis[3,7]. Mathematically for a helix, they can be expressed like this:

Eq. 18 $$\kappa = \frac{r}{(r^2+c^2)}$$

Eq. 19 $$\tau = \frac{c}{(r^2+c^2)}$$

For the collagen triple helix, κ = 0.9744 and τ = 0.5914. In order to calculate the curvature and torsion for the simulated tropocollagen, the coordinates were found using VMD and an approximate axial rise and diameter were calculated. For this simulated tropocollagen, the approximate diameter is 1.55 nm and the approximate axial rise is 3.18 nm. Therefore, the κ = 0.9237 and τ = 0.6395. The approximate axial rise is slightly off from the reported value of 2.86 nm, however, there have been some discrepancies regarding this value. Experimental studies have shown that different types of collagen have different values for the axial rise. This arises from the fact that the amino acid sequence for collagen is not merely a repeating tripeptide of GLY-PRO-HYP. There is much variability, with some collagen types having regions with multiple axial rises along the same tropocollagen[25]. The curvature is approximately the same, however the torsion is noticeably different. This result may be due to the short length of the tropocollagen, which may not be long enough for the strands to twist tightly around the axis, so the torsion is higher.

Next, we checked the distance between the side chain beads of a PRO residue that of a HYP residue on one strand. Similar to the curvature and torsion, the coordinates of

the side chain beads were found using VMD, and a simple 3-dimensional distance formula was applied.

Eq. 20 $$d = \sqrt[2]{((x_{PRO} - x_{HYP})^2 + (y_{PRO} - y_{HYP})^2 + (z_{PRO} - z_{HYP})^2)}$$

For this simulated tropocollagen, the distance was approximately 0.55 ± 0.08 nm, which is close to the reported value of 0.5 nm[4]. This indicates that the hypothesis of increasing the force constant of the angle in order to achieve the reported value between the PRO and HYP side chain beads is correct. This can be further optimized in future studies.

6.2 Interaction Counts

To find out whether or not the collagen triple helix did uncoil after 320 ns, we calculated the interaction counts. For this study, an interaction count is when two beads on different strands are within the LJ cutoff of 1.2 nm. Any distance less than the cutoff would result in the two beads interacting following the LJ potential, whereas any distance greater than the cutoff would result in the two beads not interacting at all. The calculations were done by creating a MATLAB code that reads the positions of each of the beads on one strand, and then finds the distance to the beads on the other strands. In order to figure out if the various strands are interacting, the distance was checked against the cutoff. The interactions for the triple helix would occur between strands 1 and 2, 2 and 3, and 3 and 1, resulting in three separate interaction counts. An average was taken over time to find out the average interaction count for each strand pair.

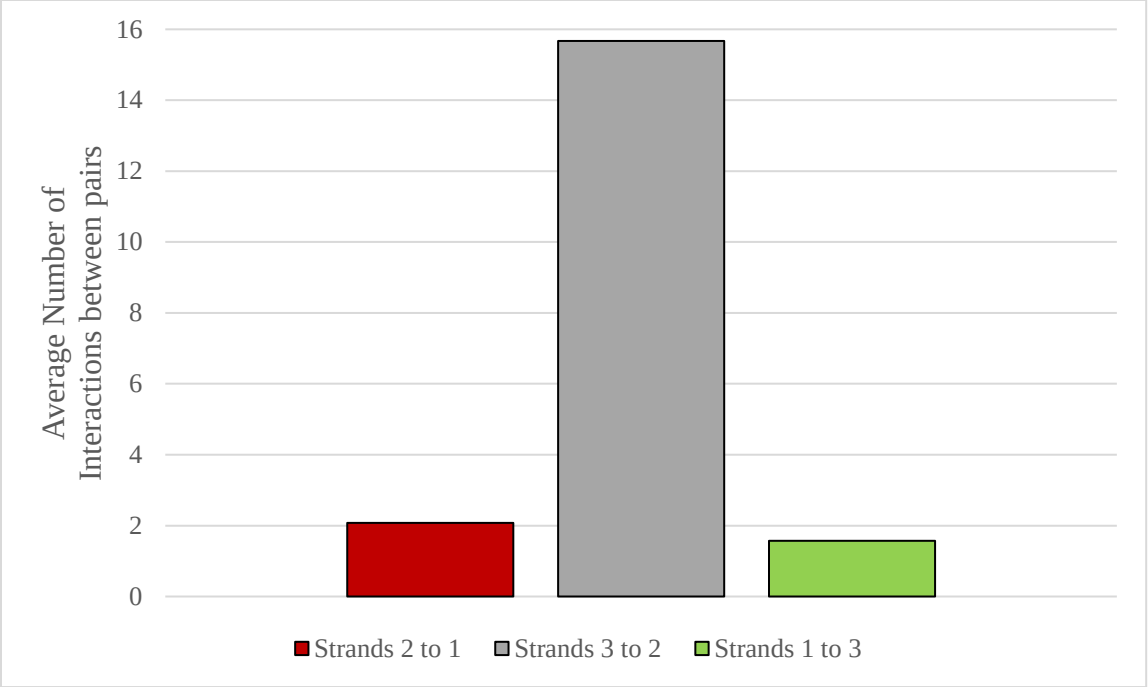

Figure 23: The average number of interactions between the strand pairs. The highest consistently occurs between strand 2 and 3. On the other hand, strand 1 is minimally interacting with either strand 2 or strand 3.

For the triple helix, strands 3 and 2 had the highest average interaction count throughout the simulation, with approximately sixteen interaction counts. This corresponds to the parallel orientation of these two strands, as shown by figure 16. Therefore, these two strands are interacting throughout the length of the strand. Strand 1 minimally interacts with the other two strands, as shown by figure 16. This strand is only interacting with the other two at the ends, which is why the average interaction count is approximately two. These results can lead to the conclusion that the triple helix has partially uncoiled.

The same logic was then applied to the microfibril system. The code was modified for this system so that it would count the interaction between strand 1 and strands 2-18, etc. This results in eighteen different average interaction counts over the duration of the simulation.

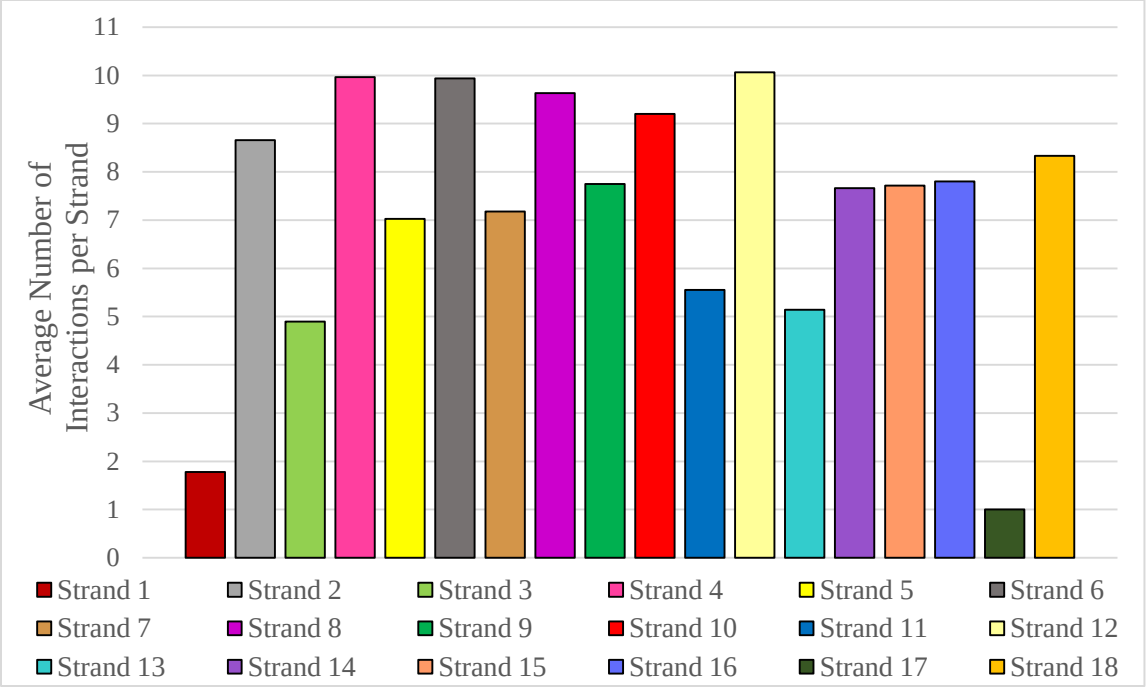

Figure 24: The average interaction counts for each of the 18 interactions. Each bar in the histogram refers to the strand to which the pairs were taken -- ie. Strand 1 implies the interactions between sstrands2 to 1, 3 to 1, etc.

A similar pattern appears for the microfibril system as compared to the tropocollagen system. Strand 17 has the fewest interactions with the others, and strand 1 has the second fewest. The strands with less than eight interactions with the other strands are 3, 5, 7, 9, 11, 13, 14, 15, 16, and 18. The strands with more than eight interactions are 2, 4, 6, 8, 10, and 12. These two groups have less than the maximum average interaction counts from the tropocollagen system of fifteen.

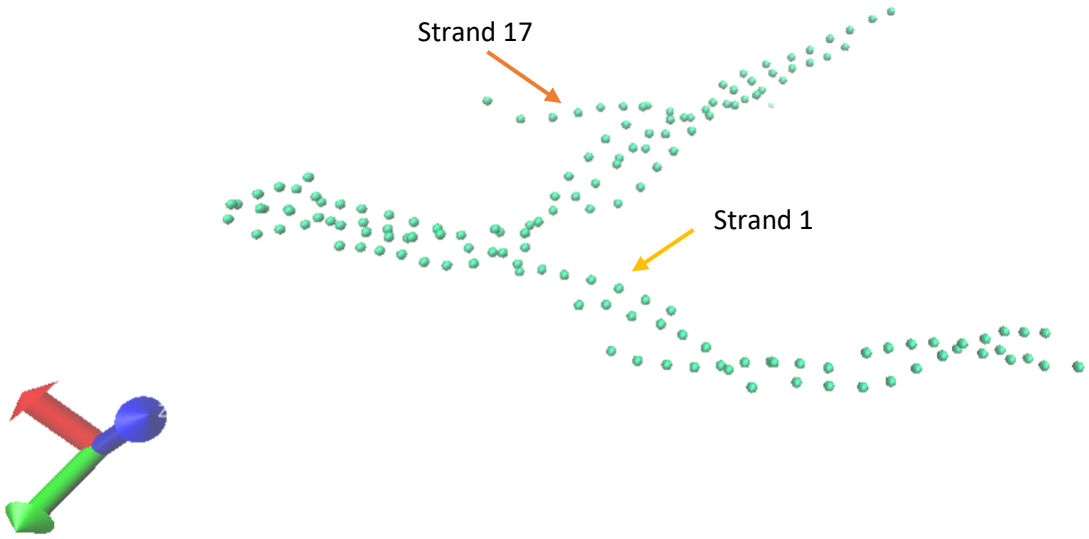

Figure 25: The microfibril system after 1.1 ns, showing only the GLY backbone beads for clarity. The orange arrow points to what appears to be strand 17, as it is only interacting at one end. The yellow arrow is pointing to what appears to be strand 1, as it is only interacting at the two ends.

This would imply that the mechanism of formation for this system is not the strands forming 6 different tropocollagens and then bundling into a microfibril. But rather, these 18 strands are twisting around each other into a microfibril-like structure. In figure 25, observing only the GLY backbone beads, we can see that the various strands are only in an elongated triple helix-like Y-shaped fiber, rather than the packing of 6 triple helices into a microfibril. These results could mean that a partially uncoiled tropocollagen replicated five more times would result in a randomized self-assembly of the individual peptide strands.

One possibility is that the microfibril system would need to run for longer than 1.1 μs, to perhaps 2.0 μs, to get a proper microfibril. However, this seems unlikely, considering the strands are not forming proper tropocollagens before bundling into a microfibril. To get a proper microfibril, the tropocollagen may need to be more coiled, as

it appeared to be in about 120 ns into the first simulation. This process would need to be further optimized in future studies, in order to form a stable tropocollagen that does not coil, even partially, and to form the microfibril. One such optimization method could be to utilize SMD in order to force the tropocollagens to form a microfibril. This may be closer to the biological pathway of collagen formation, as various "helper" molecules, ribosomes, enzymes, and even the propeptides at the ends of the collagen peptide strands aid in the formation of triple helices and fibrils. We are currently in the process of simulating this microfibril system up to 2.0 μs, as well as running seven more seeds to determine if this mechanism is a reoccurring phenomenon.

Chapter 7: Conclusions

In this study, we have simulated three strands made up of $[GLY\text{-}PRO\text{-}HYP]_{27}$ in order to form a triple helix-like structure. This structure was then characterized using the parametric equations for a helix, with a curvature $\kappa = 0.9237$ and a torsion $\tau = 0.6395$, which are extremely similar to the ones calculated using the reported values of a collagen triple helix. We also calculated the distance between the PRO side chain beads on one strand with the HYP side chain beads on another strand. The distance was found to be 0.55 nm, which is extremely similar to the reported 0.5 nm value for a collagen triple helix. Therefore, we were able to characterize the triple helix using mathematical equations. However, the triple helix appeared to have partially uncoiled.

Then, we went on to calculate the interaction count by comparing the distance between beads on different strands with the LJ cutoff value of 1.2 nm. When we calculated the average interaction counts between the strands for the triple helix, we found that only strands 2 and 3 had interactions throughout the length of the strand. The corresponds to the VMD image of the tropocollagen at 320 ns, where these two strands appear to be twisting around each other and strand 1 is interacting with them at the ends. A similar story appeared for the microfibril system, where strand 1 and 17 had the fewest interactions, a result that corresponded to the VMD image. Therefore, it appears that the individual strands are bundling to form a microfibril-like structure, or an elongated triple helix-like structure. It appears to not form a properly coiled tropocollagen, with a more stable triple helix. It is unclear whether or not this is due to the length of the strands. Future studies can explore this by simulating a much longer peptide strand, around 50 residues, in order to see if the same sort of coiling and bundling mechanism occurs.

Chapter 8: Future Work

Future studies can optimize the results found in this study, by lengthening the peptide strand, tuning the force parameters, utilizing SMD, etc. Once the interactions are better understood within a microfibril, this MARTINI coarse grained scheme can be mapped to an “ultra-coarse grained” scheme that can simulate hundreds of tropocollagens to form gels and much larger networks. A larger scale could also explore the mechanisms of deterioration of the collagen fibers.

Bibliography

1. Allen, M.P.; Tildesley, D.J. *Computer Simulation of Liquids*; Clarendon Press: Oxford, 1989.
2. Attig, Norbert; Binder Kurt; Grumüller, Helmut; Kremer, Kurt (Eds). *Computational Soft Matter: from Synthetic Polymers to Proteins*; NIC-Directors: Jülich, Germany, 2004.
3. Bahrami, Amir Houshang; Jalali, Mir Abbas. Vesicle deformations by clusters of transmembrane proteins. *J. Chem. Phys*. **2011**, *134*.
4. Brinckmann, Jurgen; Notbohm, Holger; Müller, P.K. Collagen: primer in structure, processing and assembly. *Top Curr. Chem*. **2005**, *247*.
5. Buehler, Markus J. Atomistic and continuum modeling of mechanical properties of collagen: elasticity, fracture, and self-assembly. *J. Mater. Res.* **2006**, *21*, 1947-1961.
6. Buehler, Markus J. Nature designs tough collagen: explaining the nanostructure of collagen fibrils. *PNAS*. **2006**, *103*, 12285-12290.
7. de Carmo, Mantredo P. *Differential Geometry of Curves and Surfaces*; Prentice-Hall: Englewood Cliffs, New Jersey, 1976.
8. Frenkel, Daan; Smit, Berend. *Understanding Molecular Simulation: From Algorithms to Applications*; Academic Press: New York, 2001.
9. Forever Living Dream. https://foreverlivingdream.com/2012/02/10/what-is-your-arterial-age (accessed June 2017).
10. Ganceviciene, Ruta; Liakou, Aikaterini L.; Theodioridis, Athanasios; Makrantonaki, Evgenia; Zouboulis, Christos C. Skin anti-aging strategies. *Dermatoendocrinol*. **2012**, *4*, 308-319.

11. Gautieri, Alfonso; Russo, Antonio; Vesetini, Simone; Redaelli, Alberto; Buehler, Markus J. Coarse-grained model of collagen molecules using an extended MARTINI force field. *J. Chem. Theory Comput.* **2010**, *6*, 1210-1218. 4
12. Gautieri, Alfonso; Uzel, Sebastien; Vesentini, Simone; Redaelli, Alberto; Buehler, Markus J. Molecular and mesoscale mechanisms of osteogenesis imperfecta disease in collagen fibrils. *Biophys. J*. **2009**, *97*, 857-865.
13. Gautieri, Alfonso; Vesentini, Simone; Redaelli, Alberto; Ballarini Roberto. Modeling and measuring visco-elastic properties: from collagen molecules to collagen fibrils. *Int. J. Nonlinear Mech*. **2013**, *56*, 25-33.
14. Gautieri, Alfonso; Vesetini, Simone; Redaelli, Alberto; Buehler, Markus J. Hierarchial structure and nanomechanics of collagen microfibrils from the atomistic scale up. *Nano Lett*. **2011**, *11*, 757-766.
15. Ghodsi, Hossein; Darvish, Kurosh. Characterization of the viscoelastic behavior of a simplified collagen microfibril based on molecular dynamics simulations. *J. Mech. Behav. Biomed. Mater*. **2016**, *63*, 26-34.
16. GROMACS. http://www.gromacs.org (accessed Aug 2016).
17. Kadler, K. F.; Holmes, D. F.; Trotter, J.A.; Chapman, J.A. Collagen fibril formation. *Biochem. J*. **1996**, *316*, 1-11.
18. Kmiecik, Sebastian; Gront, Dominik; Kolinski, Michael; Wieteska, Lukasz; Dawid, Aleksandra Elzbieta; Kolinski, Andzej. Course-grained protein models and their applications. *Chem. Rev*. **2016**, *116*, 7898-7936.
19. Lodish, Harvey; Bark, Arnold; Zipursky, S. Lawrence; Matsudaira, Paul; Baltimore, David; Darnell, James. *Molecular Cell Biology*; W.H. Freeman: New York, 2000.

20. Marrink, Siewart-Jan; Risselada, H. Jelger; Yefimov, Serge; Tieleman, D. Peter; de Vries, Alex H. The MARTINI force field: coarse grained model for biomolecular simulations. *J. Phys. Chem. B.* **2007**, *111*, 7812-7824.
21. Monticelli, Luca; Kandasamy, Senthil K.; Periole, Xavier; Larson, Ronald G.; Tieleman, D. Peter; Marrink, Siewart-Jan. The MARTINI coarse-grained force field: extension to proteins. *J. Chem. Theory and Comput.* **2008**, *4*, 819-834.
22. Na, George C.; Butz, Linda J.; Carroll, Robbert J. Mechanism of *in vitro* collagen fibril assembly. *J. Biol. Chem.* **1986**, *261*, 12290-12299.
23. Nonlinear Regression and Curve Fitting. http://www.nlreg.com (accessed May 2017).
24. Oregon State University. http://www.sciencedaily.com/releases/2006/11/061103104048.htm (accessed July 2017).
25. Orgel, Joseph P. R. O.; Persikov, Anton; Antipova, Olga. Variation in the helical structure of native collagen. *PLoS ONE*. **2014**, *9.*
26. Sakai, Lynn Y.; Keene, Douglas R.; Morris, Nicholas P.; Burgeson, Robert E. Type VII collagen is a major structural component of anchoring fibrils. *J. Cell Biol*. **1986**, *103*, 1577-1586.
27. San Antonio, James D.; Schweitzer, Mary H.; Jensen, Shane T.; Kalluri, Raghu; Buckley, Michael; Orgel, Joseph P. R. O. Dinosaur peptides suggest mechanism of protein survival. *PLoS ONE*. **2011**, *6.*
28. Sandhu, Simarpreet V.; Gupta, Shruti; Bansal, Himanta; Singla, Kartesh. Collagen in Health and Disease. *J. Orofac. Res.* **2012**, *2*, 153-159.

29. Scott, John E. Proteoglycan-fibrillar collagen interactions. *Biochem. J.* **1988**, *252*, 313-323.

30. Tiaho, François; Recher, Graëlle; Rouèdee, Dennis. Estimation of helical angles of myosin and collagen by second harmonic generation imaging microscopy. *Opt. Express*. **2007**, *15*, 12286-12295.